IJMF, Iranian Journal of Materials Forming, Vol. 2, No. 1, pp 51-61
Printed in The Islamic Republic of Iran, 2015

Stacking Fault Energy and Microstructural Insight into the Dynamic Deformation of High-Manganese TRIP and TWIP Steels

A. Khosravifard[1*], M. M. Moshksar[2] and R. Ebrahimi[2]

[1]Department of Materials Science and Engineering, College of Chemical and Metallurgical Engineering, Shiraz Branch, Islamic Azad University, Shiraz 71955, Iran
[2] Department of Materials Science and Engineering, School of Engineering, Shiraz University, Shiraz 71348, Iran

Abstract: The dynamic behavior of three high manganese steels with very different stacking fault energy (SFE) values (4-30 mJ/m^2) were studied using high strain rate torsional tests. The hot-rolled microstructure of the steel with the lowest SFE of 4 mJ/m^2 consisted of a duplex mixture of austenite and ε-martensite, but those of the other two steels were fully austenitic. The deformed microstructures were studied by optical and electron microscopy. The quasi-static deformation of the low-SFE steel was accompanied with profuse martensitic transformation. However, when this steel was deformed at high strain rates (> 500 /s), martensite formation was reduced due to the adiabatic temperature rise and the increased SFE of the steel. The deformation of the steel with moderate SFE of 18 mJ/m^2 at all the tested strain rates was mainly controlled by the formation of mechanical twins that was leading to an excellent ductility of about 55% even at the highest strain rate of ~1700 /s. In contrast, dynamic deformation of the steel with the highest SFE of 30 mJ/m^2 led to the appearance of some shear bands. This was ascribed to the decreased twinning and work hardening rate in this steel. Finally, the topographic studies showed that the fracture surface of the low-SFE steel contained relatively larger cleavage areas and smaller dimples suggesting a relatively more brittle fracture. This was related to the presence of brittle ε and α` martensite phases in this steel.

Keywords: Stacking fault energy, High manganese, TRIP, TWIP, High strain rate

1. Introduction

Advanced high strength steels (AHSS) have been increasingly considered in the automotive industries in order to increase the crash-worthiness while reducing the total weight and fuel consumption [1]. Two modern subcategories of AHSS, i.e. transformation induced plasticity (TRIP) and twinning induced plasticity (TWIP) steels have attracted great attention due to their superior mechanical properties. Depending on the manganese content of the steel, TRIP steels are categorized as low and high alloy. Low-Mn TRIP steels consist of a mixture of austenite, ferrite and bainite [1, 2], while in high-Mn TRIP steels, a fully austenitic microstructure may exist at room temperature [3]. Plastic deformation of a TRIP steel is accompanied with martensitic transformation of austenite in the form of $\gamma \rightarrow \varepsilon$ or $\gamma \rightarrow \varepsilon \rightarrow \alpha'$ [3]. However, in case of a TWIP steel, due to presence of a high concentration of manganese (usually >15 wt%), austenite (γ) phase remains stable down to room temperature. In the course of deformation, mechanical twins are formed within the austenitic grains of a TWIP steel [4, 5]. Mechanical twins in TWIP steels are generated as the result of movement of Shockley partial dislocations on successive {111} planes of austenite [6]. The dominant deformation mechanism in high-Mn steels (martensitic transformation, mechanical twinning or slip by dislocation glide) depends on the stacking fault energy

Received by the editors March 7, 2015; Revised March 31, 2015 and Accepted April 1, 2015.
*Corresponding author (khosravifard@iaushirazu.ac.ir)

(SFE). In order to control the SFE, a few percent of certain alloying elements, mainly aluminum and silicon, may also be added to the composition of the steel [5].

Lee et al. [7] studied the quasi-static mechanical response of a fine-grained low-Mn TRIP steel containing 0.05 C-6.15 Mn-1.5 Si. It was seen that the ultimate tensile strength (UTS) and ductility (elongation) of different specimens which were annealed at various temperatures were between 1000-1350 MPa and 7-20%, respectively. A higher ductility of up to ~40% was reported for another low-Mn TRIP steel containing 0.1 C-7.1 Mn-0.13 Si [8]. Considerably higher values of ductility (up to ~70%) were reported by Grassel et al. [9] for a high-Mn TRIP steel containing 20 Mn-3 Al-3 Si. The combination of high strength and ductility in TRIP steels has been ascribed to the generation of martensite lathes which strengthen the steel and at the same time prevent the occurrence of macroscopic instability [10]. In case of TWIP steels, mechanical twins play a similar role that leads to excellent hardening and ductility work. According to Bouaziz et al. [11], at quasi-static strain rates and room temperature, UTS of TWIP steels fall in the range 700-1500 MPa and the values of ductility are between 30-60%. Curtze and Kuokkala [12] studied three high-Mn TWIP steels with manganese concentrations of 25-28%. They found that the quasi-static work hardening rate $(d\sigma / d\varepsilon)$ of the steels remains high up to true strains as large as ~0.4. Microstructural studies showed that after a critical strain, the rate of generation of mechanical twins and their influence on the work hardening of the steel is decreased [13, 14]. In some recent studies, Lebedkina et al. [15] and Chung et al. [16] conducted experiments at different strain rates in quasi-static regime and attained negative strain rate sensitivity for high-Mn TWIP steels. This observation has been related to the dynamic strain aging (DSA) which is also known as the Portevin-Lechatlier effect.

While extensive studies have been performed on the quasi-static behavior of TRIP and TWIP steels, there are only a few studies regarding their dynamic behavior. Grassel et al. [9] performed compressive and tensile split-Hopkinson experiments on steels containing 15-30 wt% Mn. It was found that increasing the manganese content of the steel up to 25% leads to decreased strength and increased ductility at high strain rates of up to ~1000 /s. Sun et al. [17] measured a ductility of ~30% in tensile dynamic experiments which were performed on a TRIP800 steel. Sahu et al. [18] performed compressive Hopkinson experiments on high-Mn steels and found that the transformation of austenite to martensite may be prevented as the result of adiabatic temperature rise. The high strain rate torsional behavior of a series of high-Mn steels with manganese contents of 20-24 wt% have been studied by the present authors using a torsional split-Hopkinson setup. The interpretation of the dynamic mechanical behavior of the studied steels has been mentioned in previous publications [19, 20, 21]. However, the microstructural evolutions during the high rate deformation of high-Mn steels and the influence of stacking fault energy and its variations during the deformation have been rarely studied.

In the present work, high-Mn steels with different values of SFE have been studied in the high strain rate regime. The microstructural changes are discussed in relation with the SFE values and their alterations during the dynamic deformation. The topographic features of the fracture surfaces of the deformed specimens are also surveyed.

2. Experimental Procedure

A high strain rate torsional setup was designed and constructed to perform the dynamic tests (Fig. 1). Initially, the incident bar is tightly clamped at the location of clamp 2. The motor and gearbox system twist the end of the bar up to a desired angle. Thus, a certain value of torque is stored in the incident bar. Then, clamp 1 is tightened and clamp 2 is rapidly released. As the result, the stored torque is released and a torsional wave travels towards the specimen. By measuring the generated torsional pulses on the incident and transmitter bars, the instantaneous values of stress and strain in the specimen are calculated. Details of

the specimen fabrication and testing procedure are described in the previous work [19]. The experimental materials were three high-Mn steels with the chemical compositions mentioned in Table 1. The steels were designated based on their carbon content, i.e. HC (high-carbon), MC (medium carbon) and LC (low-carbon). Prior to the fabrication of the specimens, the hot deformation behavior of the steels were studied using hot compression tests [22]. Thus, the values of the critical strain for the occurrence of dynamic recrystallization were determined at various temperatures and strain rates. Utilizing the results of hot deformation experiments, the steel slabs were firstly homogenized at a temperature of 1100-1150 ˚C and were consequently hot rolled from an initial thickness of 43-47 mm to a final thickness of 18 mm. After rolling, the slabs were quenched from the temperature of ~850 ˚C to minimize grain growth and possible carbide precipitation.

Table 1. Chemical compositions of the studied steels (wt. %).

Alloy Designation	% C	% Mn	% Al	% Si	% Fe
HC steel	0.49	21.6	0.8	2.7	Bal.
MC steel	0.16	24.1	0.91	0.54	Bal.
LC steel	0.07	20.1	0.59	2.1	Bal.

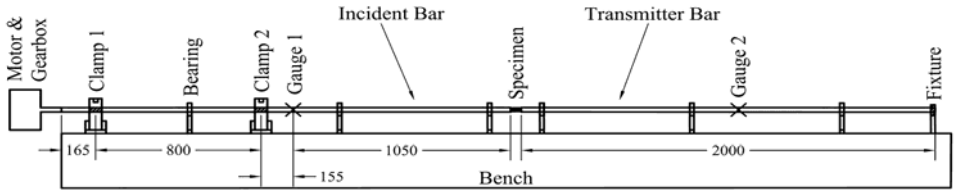

Fig. 1. Schematic representation of the torsional testing setup used for dynamic experiments.

In order to perform microstructural studies, the dynamically deformed specimens were cold mounted using an epoxy resin-hardener mixture. Then, in order to reach the middle gauge zone, one of the end flanges were completely removed using mechanical polishing (Fig. 2). Final polishing was performed using 0.05 μm diamond paste. Prior to microscopy, the specimens were etched in 10% Nital. In case of color metallography, the specimens were re-etched using Braha's sulfamic acid reagent. A Nikon optical microscope and a TESCAN VEGA scanning electron microscope (SEM) were used for microscopic studies. In order to study the fractographic features of the deformed specimens, ultra-sonic cleansing of the fracture surface was done using acetone and the fractographs were acquired using a Cambridge S-360 SEM. X-ray diffraction (XRD) patterns of the specimens were prepared using a Bruker D8 Advance Diffractometer.

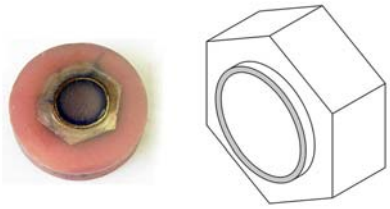

Fig. 2. The transverse cross-section of the dynamically deformed thin cylindrical specimens used for microstructural studies.

3. Results and Discussion

3.1. Hot-rolled microstructures

The microstructures which were obtained after hot rolling of the three steels are demonstrated in Fig. 3. Prior to the torsional tests, the microstructure of HC and MC steels were single phase austenitic, but that of the LC steel consisted of a duplex mixture of austenite and martensite. The XRD pattern of the LC steel

showed that the martensite phase in the initial microstructure was ε-martensite with hexagonal close packed (hcp) crystal structure (Fig. 4). Thus, it can be seen that some of the austenite phase in the microstructure of the LC-steel transforms into ε-martensite upon cooling to room temperature. This is due to the very low value of SFE in this steel. Calculations of the SFE will be presented in the next section. The XRD patterns also proved the single phase austenitic microstructures in the HC and MC steels (Figs. 4a and b).

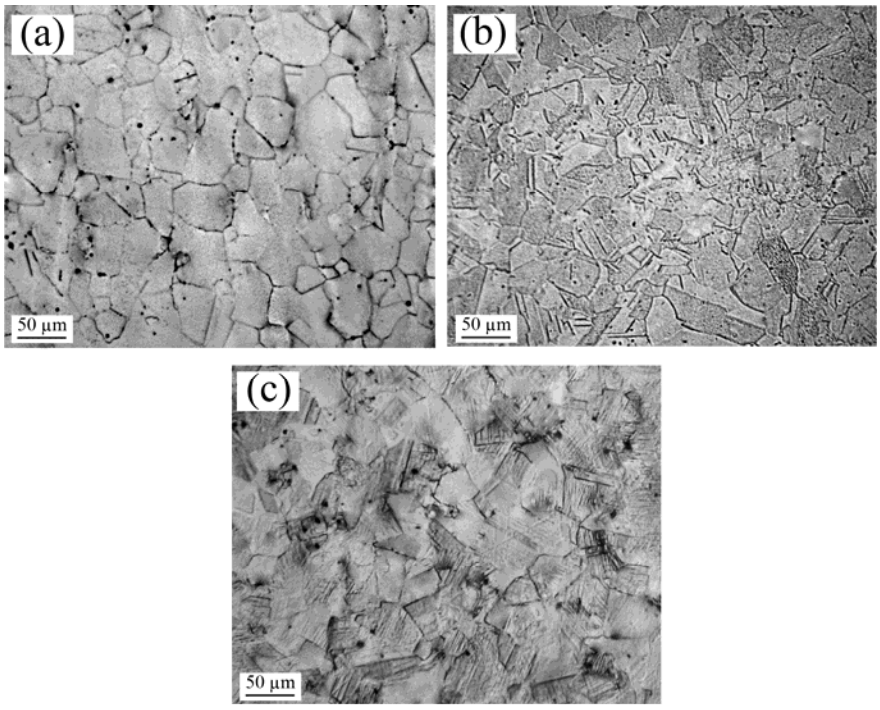

Fig. 3. Optical micrographs of (a) HC steel, (b) MC steel and (c) LC steel after hot rolling.

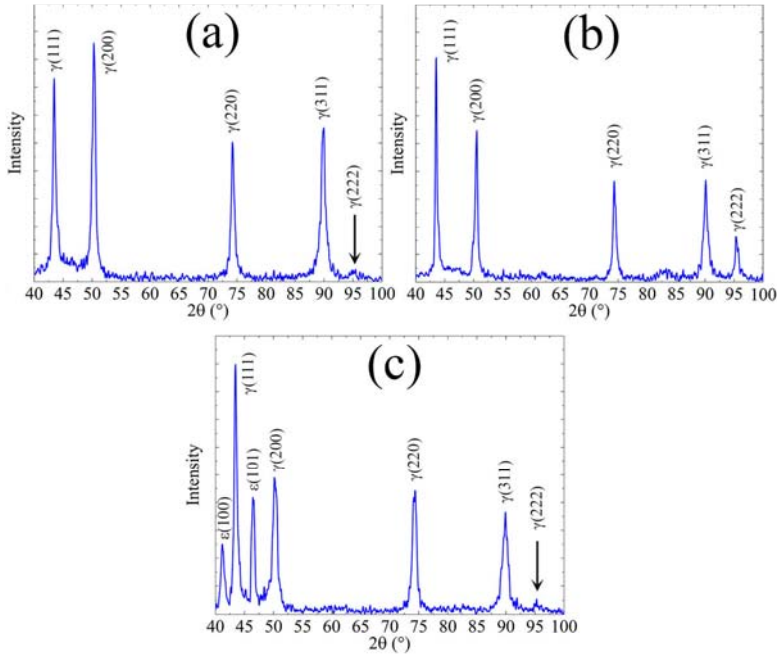

Fig. 4. XRD patterns of (a) HC steel, (b) MC steel and (c) LC steel after hot rolling.

3.2. Stacking fault energy calculations

The stacking fault energy (SFE) of the three steels were calculated using the thermodynamical approach of Olson and Cohen [23]:

$$SFE = 2\rho_s \Delta G^{\gamma\to\varepsilon} + 2\sigma^{\gamma/\varepsilon} \quad (1)$$

where ρ_s is the molar density of atoms on close-packed {111} planes, $\sigma^{\gamma/\varepsilon}$ is the γ/ε interfacial energy per unit area, and $\Delta G^{\gamma\to\varepsilon}$ is the molar free energy change during austenite to martensite transformation. The latter term was considered as a function of temperature for different components of the studied steels [19]. As the result, the contribution of different alloying elements and thus the SFE of the three steels at various temperatures could be measured (Fig. 5). The contribution of each separate alloying element is for instance shown for HC steel (Fig. 5a). Obviously, high carbon content of this steel has played a major role in increasing its SFE. Furthermore, it can be seen that as the temperature increases, Silicon is the only alloying element which lowers the SFE. Thus, this element can be considered for controlling the SFE in cases where a temperature rise is expected. The total values of SFE (considering the influences of all the alloying elements) are plotted on Fig. 5b for the three steels at various temperatures. The dominant deformation mechanism in each range of SFE is also superimposed on the figure. As the temperature increases, the dominant deformation mechanism of LC steel may change from martensitic transformation to mechanical twinning. This may occur at large strains during the dynamic deformation of this steel [21]. In contrast, due to higher SFE values of HC and MC steels, martensitic transformation is not expected during deformation of these steels at room temperature and above.

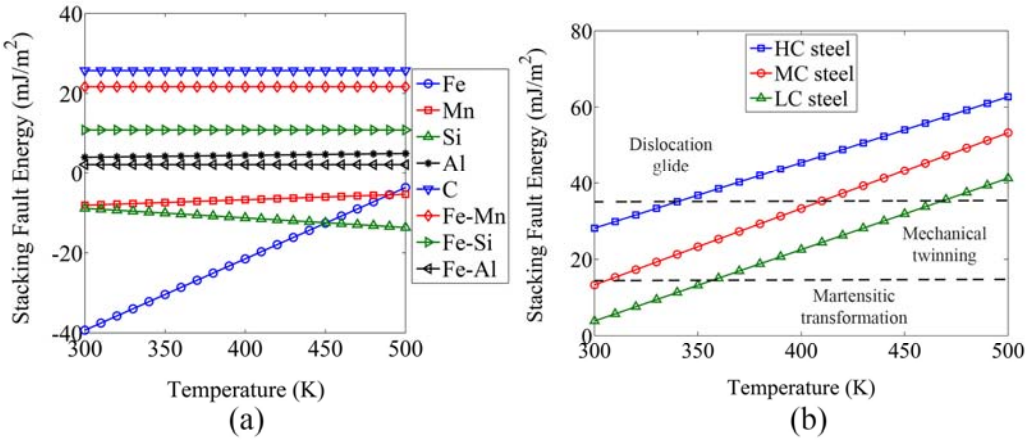

Fig. 5. Stacking fault energy as (a) the contribution of separate alloying elements of HC steel, (b) the resultant values for HC, MC and LC steels.

3.3. High strain rate torsional tests

Different values of strain rate in the range of ~500-1700 /s were reached in testing different specimens with various gauge lengths. The resultant true stress-strain curves are demonstrated in Fig. 6. For the sake of comparison, the quasi-static stress-strain curve of each steel is also provided on the figure. Deformation of the steels at the highest strain rate of ~1700 /s, has been accompanied with the appearance of a peak stress which corresponds to the failure of the test specimen. In case of HC and MC steels, a considerable increase of the flow stress occurred as the strain rate increased to ~1000 /s. This behavior may be ascribed to the increasing influence of the viscous drag of electrons and phonons at high strain rates [24]. In contrast, the high rate deformation of LC steel showed a slightly negative strain rate sensitivity. This observation was related to various possible phenomena such as decreased deformation pulse duration and increased adiabatic temperature rise at higher strain rates. As shown in Fig. 5, in case of LC steel,

adiabatic temperature rise may lead to a change of mechanism from TRIP to TWIP. Furthermore, as discussed in a previous publication [21], the significance of impact stress in LC steel is lower than the other two steels since its flow stress is initially higher. On the other hand, as the strain rate increases, the deformation pulse duration decreases which leads to reduced rate of martensitic transformation. The above phenomena resulted in a different dynamic behavior in LC steel compared to MC and HC steels. Further explanations are available in previous publications [21, 19].

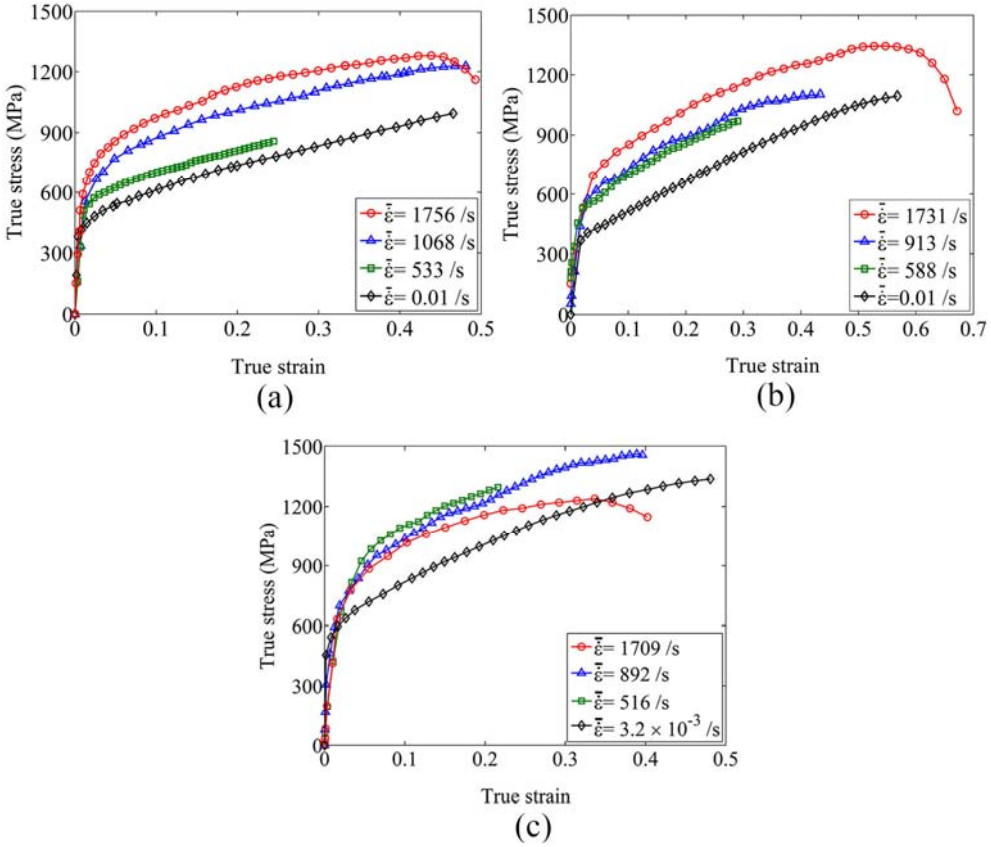

Fig. 6. True stress-strain curves obtained from high rate torsional tests on (a) HC steel, (b) MC steel, (c) LC steel.

3.4. Microstructural studies

Electron micrographs (backscatter electron) of the transverse sections of MC steel after deformation at various high strain rates are shown in Fig. 7. Mechanical twins have been generated at all the tested strain rates. As the applied strain and strain rate increased from 0.3 and 588 /s to 0.43 and 913 /s, respectively, the density of generated mechanical twins increased (Figs. 7a-c). Furthermore, the microstructures of the tested specimens at all the strain rates consist of grains in which more than one twinning system has been activated. Some of these grains have been marked by arrows on the figure. There exists an angle of about 60˚ between the activated twinning systems which is consistent with the angle between the twin planes of FCC system ({111} family). Two different arrangements could be observed for the generated twins at different strain rates. In some of the grains, the secondary twins have been stopped at the location of intersection with the primary twins (Fig. 7a). This is possibly an indication of the simultaneous activation of the two systems. However, as the strain and strain rate increased, the secondary twins have crossed over the primary twins (Fig. 7d). Thus, the twin systems have been sequentially activated which has been known as the rebound mechanism. In other words, after the activation of the primary system, the moving partial dislocations have been rebounded due to the repulsion of the primary twin boundaries and have

generated a new stacking fault region. The higher impact stresses which are applied to the specimen at higher strain rates lead to the growth of the secondary system across the primary twins.

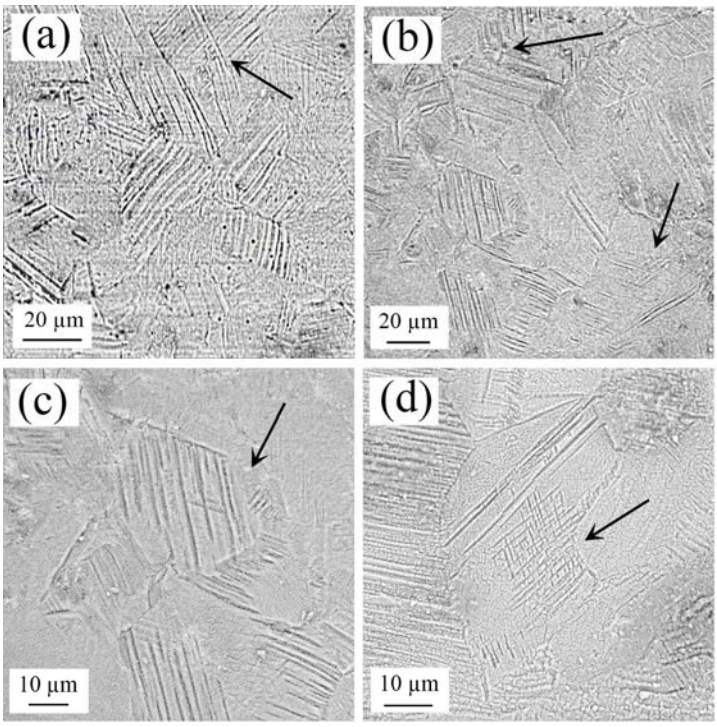

Fig. 7. Electron micrographs of the etched specimens of MC steel after applying (a) true strain of 0.3 at the strain rate of 588 /s, (b) and (c) true strain of 0.43 at the strain rate of 913 /s, (d) true strain of 0.54 at the strain rate of 1731 /s.

The high magnification band contrast map (EBSD) of the specimen of HC steel which was deformed at the strain rate of 1756 /s up to the true strain of 0.47 is shown in Fig. 8. It can be clearly seen that generated mechanical twins of this specimen have been bent. This is due to the intersection of shear bands with the mechanical twins. Because of the increased SFE of this steel due to adiabatic temperature rise of the test specimen (Fig. 5), the generation of mechanical twins is decelerated at large strains. As the result, the work hardening ability of the steel is reduced and thus, formation of shear bands during dynamic deformation of this steel seems reasonable.

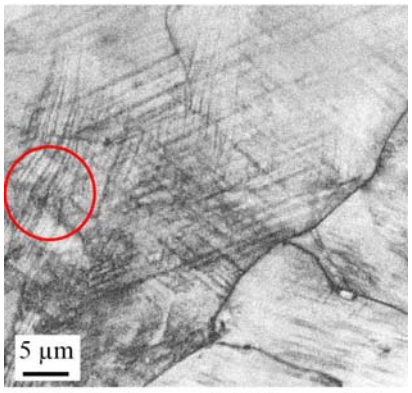

Fig. 8. Band contrast (EBSD) map of HC steel specimen deformed at the strain rate of 1756 /s to the true strain of 0.47.

The microstructure of LC steel specimen which was quasi-statically deformed up to the true strain of 0.15 is shown in Fig. 9. Due to the very low SFE of this steel (4 mJ/m^2 at room temperature), its deformation at low strain rate has been accompanied with martensitic transformation. Considering the high density of martensite laths at this strain, it can be deduced that transformation of austenite to martensite commenced at small strains. The microstructures of LC steel specimens after deformation at the strain rate of 516 /s and the quasi-static strain rate of 0.003 /s are compared in Fig. 10. The amount of martensite generated at the high strain rate is slightly less than that of the quasi-static deformation. Instead, mechanical twins are generated at the high strain rate. In some grains (marked on Fig. 10b), secondary twins have also been formed. The formation of twins at high strain rate deformation of LC steel must be due to the adiabatic temperature rise which increases the SFE of the steel (Fig. 5). The XRD pattern of the dynamically deformed specimen of LC steel shows that some α' (bct) martensite has been formed in the microstructure (Fig. 11). Comparison of this figure with Fig. 4c shows that in addition to austenite and ε-martensite, peaks of α'-martensite has also appeared in the pattern. In other words, a phase transformation in the form of $\gamma \rightarrow \varepsilon \rightarrow \alpha'$ has occurred in this specimen. The severe lattice distortion at the intersections of ε-martensite laths provides the required driving force for transformation of $\varepsilon \rightarrow \alpha'$ martensite. It must be noted that the cross-sectional area of the deformed thin-cylindrical torsional specimens is relatively small. As the result, the peaks obtained from the deformed specimen (Fig. 11) are relatively shorter than those obtained from the specimens of the hot rolled slab (Fig. 4c).

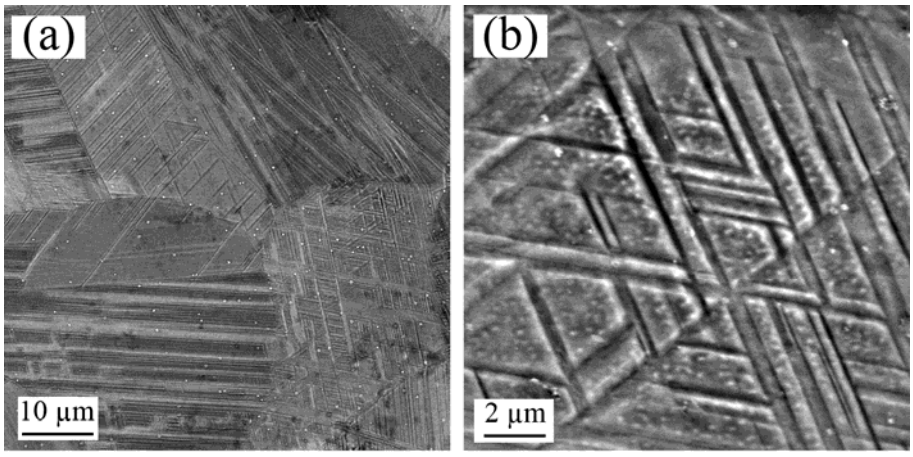

Fig. 9. Electron micrograph of LC steel specimen deformed quasi-statically to true strain of 0.15, (a) low magnification, b) high magnification.

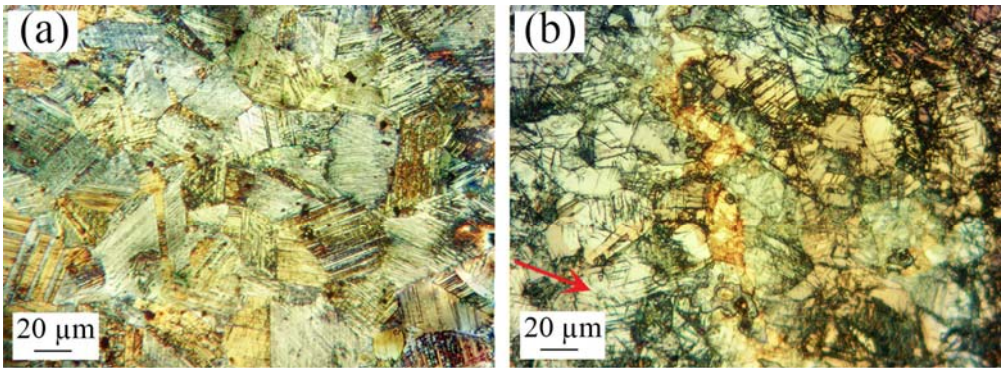

Fig. 10. Optical microstructures of LC steel after a true strain of 0.25 at the strain rate of (a) 0.003 /s and (b) 516 /s.

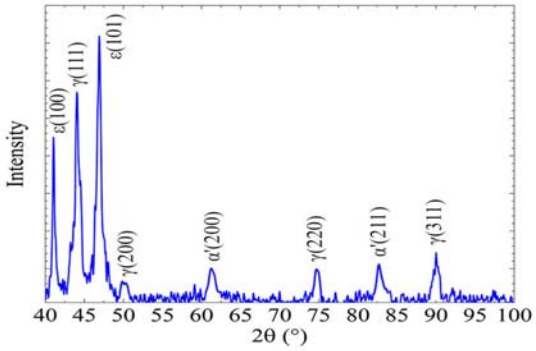

Fig. 11. XRD pattern of LC steel after dynamic deformation.

3.5. Fractography

The fracture surfaces of MC and LC steel specimens after deformation at the strain rates of ~900 and 1700 /s are demonstrated in Fig. 12. In all the specimens, dimples as indications of ductile fracture are observed. The dimples are elongated on the surface along the direction of the applied shear stress. At the strain rate of 900 /s, MC steel has experienced an almost completely ductile fracture. However, fracture surface of LC steel at the same strain rate shows some cleavage areas as indications of brittle fracture. Due to the formation of brittle phases of ε and α' martensite in this steel, the separation of austenite/martensite interfaces can lead to formation of cleavage areas. From Fig. 12, it can also be seen that the average size of dimples on the fracture surface of MC steel are larger than that of LC steel. It has been suggested that dimple size has an inverse relation to the macroscopic ductility of the material [25]. As the strain rate increases, larger cleavage areas were seen for both steels. Some of the cleavage areas are marked by arrows on the figure.

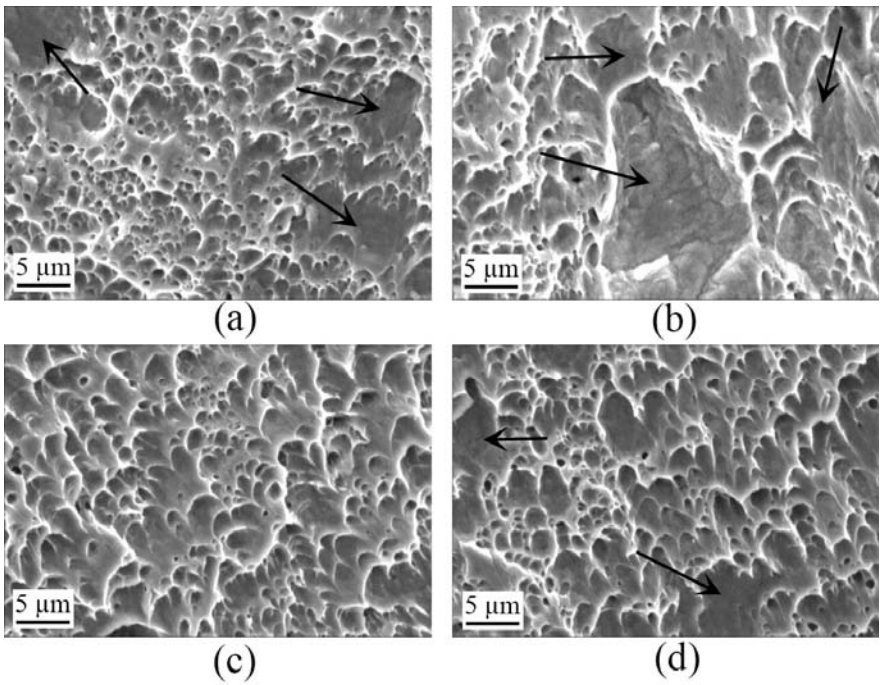

Fig. 12. Fracture surfaces of specimens deformed at the strain rates of 900 and 1700 /s, (a) and (b) LC steel, (c) and (d) MC steel.

4. Conclusion

Dynamic deformation of three high manganese steels with different stacking fault energies were studied with emphasis on the microstructural features. The following main conclusions could be drawn:

- The initial hot-rolled microstructure of the low-carbon steel (LC) consisted of a duplex mixture of austenite and ε-martensite, but for the medium-carbon (MC) and high-carbon (HC) steels, fully austenitic microstructures were obtained.
- The dominant deformation mechanism during the quasi-static deformation of the LC steel was martensitic transformation (TRIP effect) due to its very low SFE (4 mJ/m^2).
- Due to adiabatic temperature rise and increased SFE, the density of martensite laths decreased when the LC steel was deformed at high strain rates.
- The plastic deformation of MC steel was accompanied with the formation of mechanical twins (TWIP effect) at all the tested strain rates, leading to its distinctly higher ductility (~55%).
- Due to the high stacking fault energy (SFE) of the HC steel (30 mJ/m^2), formation of mechanical twins was decelerated at large strains. As the result, the work hardening ability of this steel decreased giving rise to the appearance of shear bands. The curvatures generated in the mechanical twins also confirmed the generation of bands.
- Due to the presence of brittle ε and α' martensite phases in the microstructure of LC steel, relatively larger cleavage areas and smaller dimples were observed in the fracture surface of this steel.

References

[1] V. J. Slycken, P. Verleysen, J. Degrieck, J. Bouquerel and B. C. De Cooman, Dynamic response of aluminum containing TRIP steel and its constituent phases, *Material Science and Engineering A,* 460–461 (2007) 516–524.

[2] Z. H. Cai, H. Ding, X. Xue and Q. B. Xin, Microstructural evolution and mechanical properties of hot-rolled 11% manganese TRIP steel, *Materials Science & Engineering A,* 560 (2013) 388-395.

[3] L. A. Dobrzanski and W. Borek, Thermo-mechanical treatment of Fe–Mn–(Al,Si) TRIP/TWIP steels, *Archives of Civil and Mechanical Engineering,* (2012) 299-304.

[4] S. Allain, J. P. Chateau, O. Bouaziz, S. Migot and N. Guelton, "Correlations between the calculated stacking fault energy and the plasticity mechanisms in Fe–Mn–C alloys," *Materials Science and Engineering A,* Vols. 387-389, pp. 158-162, 2004.

[5] A. Dumay, J. P. Chateau, S. Allain, M. S. and O. Bouaziz, Influence of addition elements on the stacking-fault energy and mechanical properties of an austenitic Fe–Mn–C steel, *Materials Science and Engineering A,* 483-484, (2008) 184-187.

[6] H. Idrissi, K. Renard, L. Ryeland, D. Schryvers and P. J. Jacques, On the mechanism of twin formation in Fe–Mn–C TWIP steels, *Acta Materialia,* 58, (2010) 2464-2476.

[7] S. Lee, S. J. Lee, S. S. Kumar, K. Lee and B. C. De Cooman, Localized deformation in multiphase, ultra-fine-grained 6 Pct Mn transformation-induced plasticity steel, *Metallurgical and Materials Transactions A,* 42, (2011) 3638-3651.

[8] P. J. Gibbs, E. De Moor, M. J. Merwin, B. Clausen, S. J. G. and D. K. Matlock, Austenite stability effects on tensile behavior of manganese-enriched-austenite transformation-induced plasticity steel, *Metallurgical and Materials Transactions A,* 42, (2011) 3691-3702.

[9] O. Grassel, L. Kruger, G. Frommeyer and L. W. Meyer, High strength Fe-Mn-(Al, Si) TRIP/TWIP steels development-properties-application, *International Journal of Plasticity,* 16, (2000) 1391-1409.

[10] O. Matsumura, Y. Sakuma and H. Takechi, Enhancement of elongation by retained austenite in intercritical annealed 0.4C-1.5Si-0.8Mn Steel, *Transactions of the Iron and Steel Institute of Japan,* 27 (1987) 570-579, 1987.

[11] O. Bouaziz, S. Allain, C. P. Scott, C. P. and D. Barbier, High manganese austenitic twinning induced plasticity steels: A review of the microstructure properties relationships, *Current Opinion in Solid State and Materials Science,* 15 (2011) 141-168.

[12] S. Curtze and V. T. Kuokkala, Dependence of tensile deformation behavior of TWIP steels on stacking fault energy, temperature and strain rate, *Acta Materialia,* 58 (2010) 5129-5141.

[13] J. Jin and Y. Lee, Strain hardening behavior of a Fe–18Mn–0.6C–1.5Al TWIP steel, *Materials Science and Engineering A,* 527 (2009) 157-161.

[14] Gutierrez-Urrutia and D. Raabe, Dislocation and twin substructure evolution during strain hardening of an Fe–22 wt.% Mn–0.6 wt.% C TWIP steel observed by electron channeling contrast imaging, *Acta Materialia,* 59 (2011) 6449-6462.

[15] T. A. Lebedkina, M. A. Lebyodkin, J. P. Chateau, A. Jacques and S. Allain, On the mechanism of unstable plastic flow in an austenitic FeMnC TWIP steel, *Materials Science and Engineering A,* 519 (2009) 147–154.

[16] Chung, K. Ahn, D. H. Yoo, K. H. Chung, M. H. Seo and S. H. Park, Formability of TWIP (twinning induced plasticity) automotive sheets, *International Journal of Plasticity,* 27(2011) 52-81.

[17] X. Sun, A. Soulami, K. S. Choi, O. Guzman and W. Chen, Effects of sample geometry and loading rate on tensile ductility of TRIP800 steel, *Materials Science and Engineering A,* 541 (2012) 1-7.

[18] P. Sahu, S. Curtze, A. Das, B. Mahato, K. V. T. and S. G. Chowdhury, Stability of austenite and quasi-adiabatic heating during high strain-rate deformation of twinning-induced plasticity steels, *Scripta Materialia,* 62 (2010) 5-8.

[19] A. Khosravifard, M. M. Moshksar and R. Ebrahimi, High strain rate torsional testing of a high manganese steel: Design and Simulation, *Materials and Design,* 52 (2013) 495-503.

[20] Khosravifard, M. M. Moshksar and R. Ebrahimi, Mechanical behavior of TWIP steel in high strain rate torsional test, *International Journal of Iron and Steel Society of Iran,* 9 (2012) 15-19.

[21] Khosravifard, Influence of high strain rates on the mechanical behavior of high manganese steels, *Iranian Journal of Materials Forming,* 1 (2014) 1-10.

[22] Khosravifard, A. S. Hamada, M. M. Moshksar, R. Ebrahimi, D. A. Porter and L. P. Karjalainen, High temperature deformation behavior of two as-cast high-manganese TWIP steels, *Materials Science & Engineering A,* 582 (2013) 15-21.

[23] G. Olson and M. Cohen, A general mechanism of martensitic nucleation: Part I. General concepts and the FCC-HCP transformation, *Metallurgical and Materials Transactions A,* 7 (1976). 1897-1904.

[24] G. Regazzoni, P. U. F. Kocks and P. S. Follansbee, Dislocation Kinetics at High Strain Rates, *Acta Metallurgica,* 35 (1987) 2865-2875.

[25] R. G. Xiong, R. Y. Fu, Y. Su, Q. Li, W. X. C. and L. Li, Tensile properties of TWIP steel at high strain rate, *Journal of Iron and Steel Research, International,* 16 (2009) 81-86.